Experimental study on acoustic subwavelength imaging of holey-structured metamaterials by resonant tunneling

Haijing Su, Xiaoming Zhou,[a] Xianchen Xu, and Gengkai Hu
Key Laboratory of Dynamics and Control of Flight Vehicle, Ministry of Education, and School of Aerospace Engineering, Beijing Institute of Technology, Beijing 100081, People's Republic of China

(Received 22 April 2013; revised 21 January 2014; accepted 3 March 2014)

A holey-structured metamaterial is proposed for near-field acoustic imaging beyond the diffraction limit. The structured lens consists of a rigid slab perforated with an array of cylindrical holes with periodically modulated diameters. Based on the effective medium approach, the structured lens is characterized by multilayered metamaterials with anisotropic dynamic mass, and an analytic model is proposed to evaluate the transmission properties of incident evanescent waves. The condition is derived for the resonant tunneling, by which evanescent waves can completely transmit through the structured lens without decaying. As an advantage of the proposed lens, the imaging frequency can be modified by the diameter modulation of internal holes without the change of the lens thickness in contrast to the lens due to the Fabry–Pérot resonant mechanism. In this experiment, the lens is assembled by aluminum plates drilled with cylindrical holes. The imaging experiment demonstrates that the designed lens can clearly distinguish two sources separated in the distance below the diffraction limit at the tunneling frequency. © *2014 Acoustical Society of America*. [http://dx.doi.org/10.1121/1.4868395]

PACS number(s): 43.20.Fn, 43.58.Ls, 43.20.Mv [GH] Pages: 1686–1691

I. INTRODUCTION

The diffraction effect of acoustic waves imposes a fundamental limit for the spatial resolution of imaging systems. The diffraction limit can be attributed to the absence of decaying evanescent waves in image regions that carry the fine features of objects. In the past decade, metamaterials with unusual physical properties[1,2] have been employed to achieve subwavelength images beyond the diffraction limit by enhancing transmission amplitudes of evanescent waves. Acoustic subwavelength imaging can be achieved either by the surface resonant effect in doubly negative[3] or single negative-mass metamaterials[4,5] or by the Fabry–Pérot (FP) resonant,[6,7] the near-zero mass,[8] or the resonant tunneling effects[9] in anisotropic-mass metamaterials. The advantage for the anisotropic-mass metamaterial lens is that evanescent wave amplitudes with different wave numbers can be uniformly enhanced, then the image is undistorted as a result. The reason of the uniform enhancement is that the dispersion of anisotropic metamaterials can be tailored so that the equal-frequency surface is hyperbolic or nearly flat. In such case, evanescent waves with large parallel wave numbers can be converted into propagating waves and transferred across the metamaterial lens, forming a subwavelength image. Following this mechanism, parallel stacked rigid slabs[10] or a bundle of straight brass tubes[7] have been demonstrated in experiment to produce super-resolution near-field images. For efficiently transferring evanescent waves, these lenses need to satisfy the FP resonant condition, i.e., the lens thickness equal to the integer number of half wavelength. Hence their imaging frequency is correlated to the lens thickness.

To overcome this thickness limitation, an acoustic metamaterial lens with a near-zero dynamic mass is proposed.[8] The lens is composed of parallel stacked rigid slabs with the slits partially filled by elastic layers. The clamped elastic layers produce the Drude-medium behavior;[11,12] this means that effective mass density is negative below a cutoff frequency. The zero dynamic effective mass can be realized at the cutoff frequency.[12,13] The imaging frequency, that is also the frequency where effective mass is near zero, is invariant to the lens thickness. Further studies demonstrate that this lens can also work for super-resolution imaging by the tunneling mechanism.[9] In an equivalent mass-spring periodic structure, the tunneling conditions have been derived; this requires that the lens thickness should be the integer number of half wavelength of Bloch wave in the periodic lattices. The condition means that the imaging frequency can be determined by microstructural parameters of periodic structures without the change of the lens thickness in contrast to the FP resonant lens. Motivated by previous results, in this work, we will propose a new type of lens based on holey-structured metamaterials, and the imaging features that rely on the resonant tunneling mechanism. Based on the effective medium approach, the proposed lens can be homogenized to multilayered metamaterials with an anisotropic mass density. An analytic model can be established to describe acoustic wave interaction with the lens. Finally, experimental study is conducted to verify the imaging effect of the metamaterial lens beyond diffraction limit.

II. ANALYTIC MODEL OF HOLEY-STRUCTURED LENS

A. The geometry and dispersion characteristics of the holey-structured lens

The holey-structured lens is composed of a rigid material perforated with cylindrical holes arranged into a square

[a]Author to whom correspondence should be addressed. Electronic mail: zhxming@bit.edu.cn

 0001-4966/2014/135(4)/1686/6/$30.00

lattice in the xOz plane, as shown in Fig. 1(a), where the diameter of the holes is modulated periodically along the y direction. The diameter and depth of the cylindrical holes are, respectively, $d_1 = 4d_2 = 8\,\text{mm}$ and $s_2 = 2s_1 = 20\,\text{mm}$. The period of the square array is $a = 10\,\text{mm}$ and the number of the unit cell arranged in the y direction is $N = 2$, so that the total length of the lens is 80 mm. The background medium is the air with mass density $\rho_0 = 1.25\,\text{kg/m}^3$ and sound velocity $c_0 = 343\,\text{m/s}$.

The dispersion curves are computed for the unit cell with periodic boundary conditions by meshing only the air parts, using the commercial FEM package COMSOL Multiphysics. The band structure along the ΓXMRΓ path of the irreducible Brillouin zone is shown in Fig. 1(b). The flat dispersion curve can be observed in XM and MR directions, meaning that the fundamental mode along the ΓX direction, namely inside the holes, is irrelevant to the parallel wavenumber $k_\parallel = \sqrt{k_x^2 + k_z^2}$ of incident waves. This result implies that most parts of evanescent waves can be coupled to a fundamental mode inside the holes at a unique frequency. We will explain in the following text that by coupling to the tunneling mode, evanescent waves are able to be completely transferred across the structured lens, realizing the near-field super-resolution imaging. To this end, an analytic model will be established in the next subsection to quantify transmission coefficients of evanescent waves incident on the structured lens, then to derive the tunneling condition of complete transmission for evanescent waves. It is worth noting that the tunneling mechanism is due to the standing wave resonance in a finite periodic structure and is distinct from the all-angle-negative-refraction superlens[14] based on the phase velocity matching. So the intersection between dispersion curves for the structured lens and the background air cannot be observed.

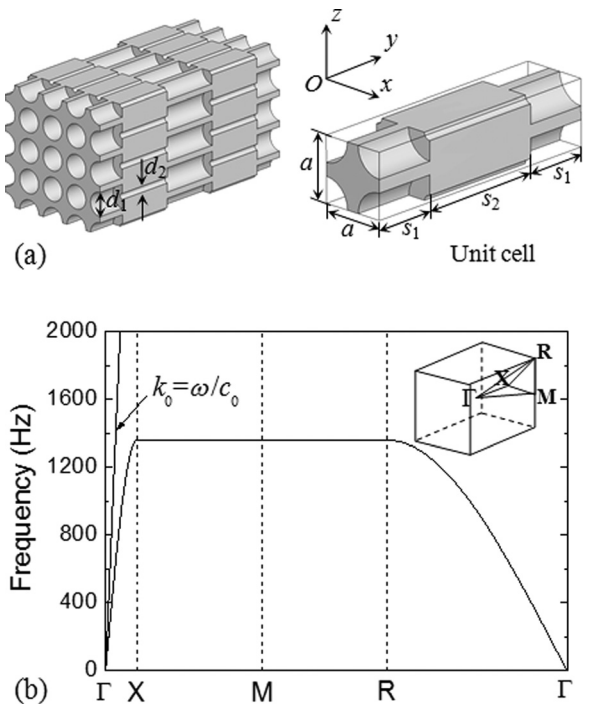

FIG. 1. (a) The model of the holey-structured lens and its unit cell; (b) the band structure of the periodic holey structure along the ΓXMRΓ path of the irreducible Brillouin zone.

B. Analytic model of the holey-structured lens

The analytic model that describes acoustic wave interaction with the studied holey structure is constructed based on effective medium approach. To proceed, we impose a limit on the lens model in that the periodicity a is far less than the operating wavelength of imaging. With this assumption, the zeroth-order longitudinal mode dominates the transmission process in cylindrical holes. As a result, the unit cell of the lens can be represented effectively by a three-layer acoustic fluid with anisotropic effective mass density as explained in Fig. 2. Effective mass density tensor $\tilde{\boldsymbol{\rho}}^{(i)}$ and sound velocity c_i for the ith layer ($i = 1,2$) are written, respectively, as[15]

$$\tilde{\boldsymbol{\rho}}^{(i)} = \text{diag}\left[\rho_i^x, \rho_i^y, \rho_i^z\right], \quad \text{with}$$
$$\rho_i^y = \rho_0 \frac{4a^2}{\pi d_i^2}, \ \rho_i^x = \rho_i^z = \infty, \tag{1a}$$

$$c_i = c_0. \tag{1b}$$

Infinite effective mass densities ρ_i^x and ρ_i^z are defined due to the fact that only the longitudinal inertial motion is allowed inside the holes. The dispersion relation for a general anisotropic-mass acoustic media is expressed as $k_x^2/\rho^x + k_y^2/\rho^y + k_z^2/\rho^z = \omega^2/\kappa$ where κ is the bulk modulus, and it becomes $k_y^{(i)} = k_0$ with $k_0 = \omega/c_0$ for the ith layer of acoustic media in the present model. The dispersion relation shows the independence on the parallel wave number $k_\parallel$; this theoretical prediction is consistent to the observation in Fig. 1(b).

For the effectively homogeneous model of the holey-structured lens, the pressure p and particle velocity v_y along the y direction in the ith region ($i = 1,2,3$) are written as

$$p = \left(A_i e^{jk_0(y-y_{i-1})} + B_i e^{-jk_0(y-y_{i-1})}\right) e^{j(k_x+k_z-\omega t)},$$
$$y_{i-1} \le y \le y_i, \tag{2a}$$

$$v_y = \frac{k_0}{\omega\rho_i^y}\left(A_i e^{jk_0(y-y_{i-1})} - B_i e^{-jk_0(y-y_{i-1})}\right) e^{j(k_x+k_z-\omega t)},$$
$$y_{i-1} \le y \le y_i, \tag{2b}$$

where $y_0 = 0$, $y_1 = s_1$, $y_2 = s_1 + s_2$, $y_3 = s = 2s_1 + s_2$, and $j = \sqrt{-1}$. When a plane acoustic wave is incident obliquely on the N three-layer units with the parallel wavenumber

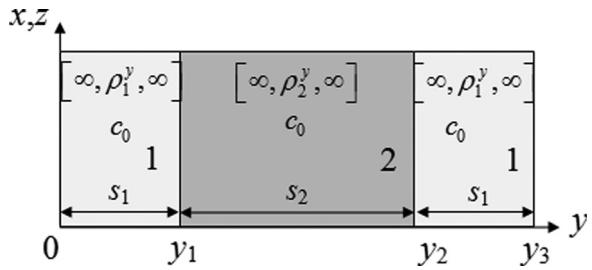

FIG. 2. The model of three-layer anisotropic acoustic fluids that effectively represents the unit cell of the structured lens under long-wavelength approximation.

$k_{\|} = \sqrt{k_x^2 + k_z^2}$, the general expression of transmission coefficient T can be expressed as

$$T(\omega, k_{\|}) = \frac{2z_0}{2z_0 \cos(Nqs) - (T_1 + T_2 z_0^2)\sin(Nqs)/\sin(qs)}, \tag{3}$$

with $z_0 = \rho_0 \omega / \sqrt{k_0^2 - k_{\|}^2}$ and

$$T_1 = i\rho_2^y c_0 \left[\frac{1}{\delta^2}\cos k_0 s_2 \sin 2k_0 s_1 + \sin k_0 s_2 \times \left(\cos^2 k_0 s_1 - \frac{1}{\delta^4}\sin^2 k_0 s_1\right)\right], \tag{4a}$$

$$T_2 = \frac{i}{\rho_2^y c_0}\left[\delta^2 \cos k_0 s_2 \sin 2k_0 s_1 + \sin k_0 s_2 \times (\cos^2 k_0 s_1 - \delta^4 \sin^2 k_0 s_1)\right], \tag{4b}$$

where $\delta = d_1/d_2$ is defined, and q is the wavenumber of the Bloch wave that propagates in the y direction and satisfies the following dispersion relation:

$$\cos qs = \cos k_0 s - \frac{1}{2}(\delta - 1/\delta)^2 \sin k_0 s_2 \sin 2k_0 s_1. \tag{5}$$

The tunneling condition corresponds to the complete transmission $|T| = 1$ for all evanescent waves with $k_{\|} > k_0$. According to Eq. (3), this condition is obtained as

$$Nqs = m\pi, \quad m = 1, 2, ..., N-1. \tag{6}$$

Note that this condition also leads to the complete transmission of propagating waves ($k_{\|} \le k_0$). Equation (6) follows the similar form to that obtained for discrete mass-spring structures.[9]

C. Analytic results and discussions

The tunneling condition for the present model ($N = 2$) reads

$$2\cos(k_0 s) = (\delta - 1/\delta)^2 \sin k_0 s_2 \sin 2k_0 s_1. \tag{7}$$

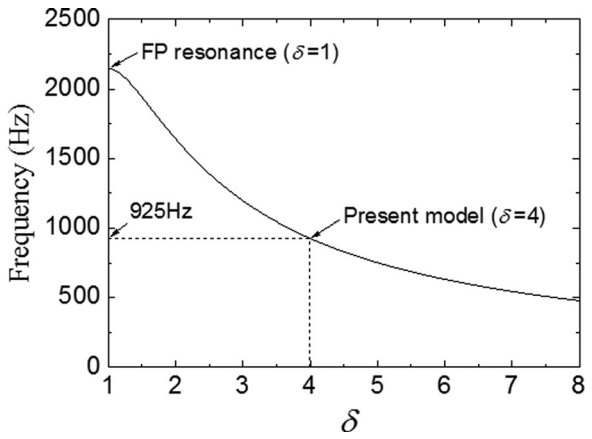

FIG. 3. The model of three-layer anisotropic acoustic fluids that effectively represents the unit cell of the structured lens under long-wavelength approximation.

If $\delta = 1$, Eq. (7) is then reduced to the FP resonant condition for which the general expression is $Nk_0 s = m\pi$.[6] In this case, the controlling parameter for the operating frequency is the lens thickness $h = Ns$. However, when the periodic holes with $\delta \neq 1$ are considered, the imaging (tunneling) frequency can be modified by the diameter ratio δ without the change of the lens thickness. In Fig. 3 is shown the tunneling frequency obtained for various δ. The tunneling frequency is always less than the FP resonant frequency and is lowered with δ deviating away from the unity. The theoretical prediction on the tunneling frequency of the studied lens ($\delta = 4$) is 925 Hz.

Figure 4 shows the contour plot of transmission amplitudes for different parallel wavenumber $k_{\|}$ and frequency of incident waves. It can be seen that incident waves, in particular evanescent waves ($k_{\|} > k_0$), can be transported with unity modulus in amplitude at the tunneling frequency 925 Hz. The result implies that the holey-structured lens could transfer subwavelength details that are characterized by large $k_{\|}$ to the output side of the lens, and produce high-resolution images in the near field.

III. NUMERICAL AND EXPERIMENTAL STUDIES ON HOLEY-STRUCTURED LENS

A. Numerical analyses on the holey-structured lens

To verify the analytic model, the transmission spectrum of normally incident waves computed by Eq. (3) are compared with numerical results by COMSOL Multiphysics, as shown in Fig. 5. It can be observed that the overall trend and magnitude between numerical and analytic results coincide very well, validating the analytic model proposed for the structured lens. But there is a small discrepancy between both results around the tunneling frequency. The reason of the deviation can be attributed to the unreasonable analytic approximation in the vicinity of abrupt changes of hole diameters where inhomogeneous wave fields prevail. As a result, the actual tunneling frequencies that result in the complete transmission turns out to be 905 Hz. As is explained before, the propagating wave vector in the lens is independent on the parallel wave number $k_{\|}$. The frequency 905 Hz is also the peak transmission frequency for any waves with

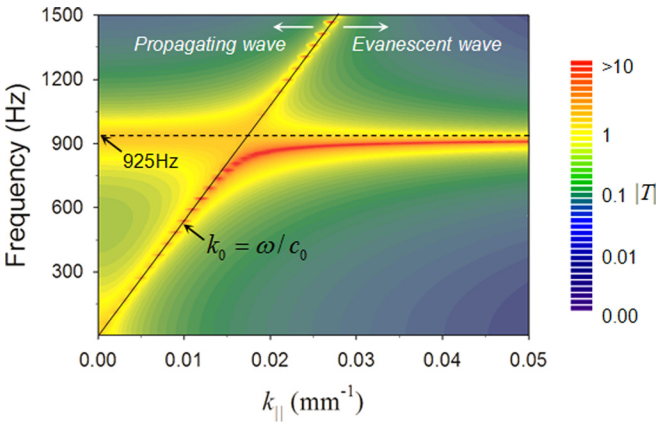

FIG. 4. (Color online) Contour plot of transmission amplitudes $|T|$ for different parallel wavenumbers $k_{\|}$ and frequencies of incident waves.

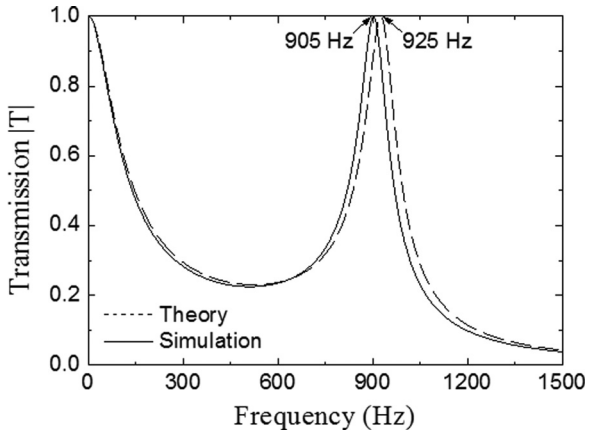

FIG. 5. Theoretical and numerical results of the transmission spectrum for acoustic waves normally incident on the holey-structured lens.

$k_{\|} > 0$, thus it will be the operating frequency for acoustic subwavelength imaging.

In Fig. 6(a) is shown the finite element model based on COMSOL Multiphysics for conceptual demonstration of the super-resolution imaging. The structured lens of a height 50 mm is placed inside a parallel waveguide with sound hard boundary settings for the top and bottom surfaces, and the waveguide is surrounded by perfectly matched layers (PML). The acoustic source emanating from a small waveguide is taken as the object. For verification of the imaging performance of the lens, pressure amplitudes will be examined in the image region that is taken to be the middle surface of the waveguide behind the lens as shown in Fig. 6(b). Simulation results for verifying imaging performance of the lens will be presented in the next subsection by comparison to the experimental results.

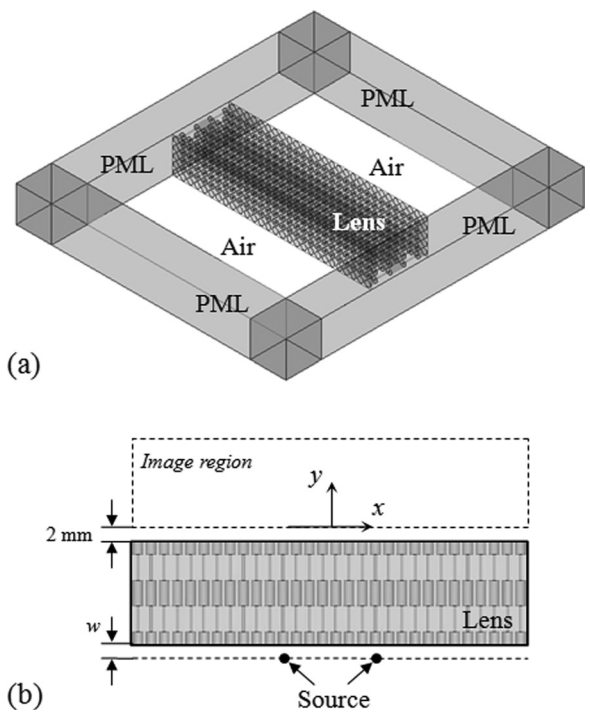

FIG. 6. (a) The finite element model for verifying imaging performance of the holey-structured lens; (b) the schematic illustration for the image region.

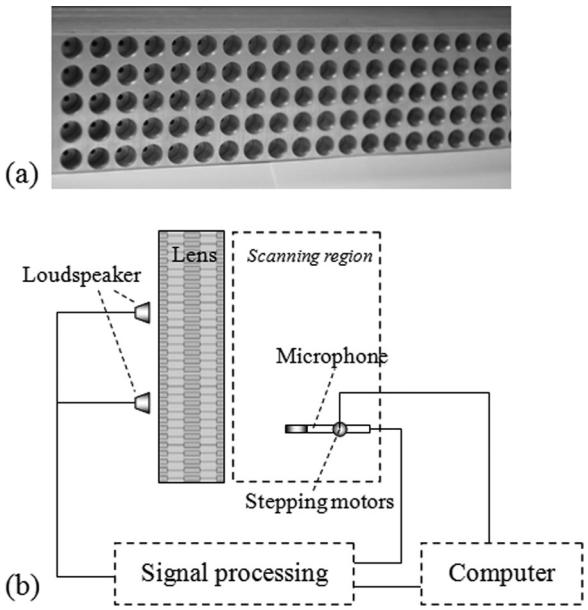

FIG. 7. (a) The fabricated sample of the holey-structured lens; (b) the scheme of the experimental setup established for verifying acoustic subwavelength imaging.

B. Experimental verification for acoustic subwavelength imaging

The holey-structured lens is assembled from five aluminum plates drilled with cylindrical holes according to the design presented in Fig. 1(a); the fabricated sample is shown in Fig. 7(a). Due to the large impedance mismatching between aluminum and air $Z_{Al}/Z_{Air} = 4.1 \times 10^4$,[16] it is reasonable to assume the aluminum lens to be rigid with respect to the air. The schematic illustration of the experimental setup established for verifying acoustic subwavelength imaging is shown in Fig. 7(b). The waveguide system for measuring acoustic response of the lens is composed of two parallel 1.0 m^2 PMMA plates of 10 mm thickness, and the distance between the plates is 50 mm. The loudspeaker is placed in front of the lens and produces continuous sine-wave signals of frequencies 905 Hz. Pressure amplitude distributions in the region behind the lens are measured by a microphone moved in 2 mm step by stepping motors. To reduce the influence of background

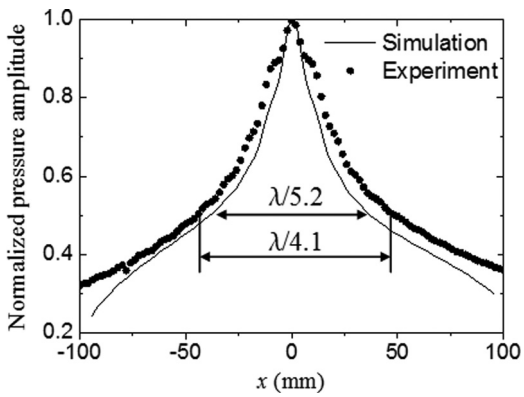

FIG. 8. Simulation and experiment results of normalized pressure amplitudes in the line taken 2 mm behind the lens when one loudspeaker operating at frequency 905 Hz is placed in front of the lens with the distance 2 mm.

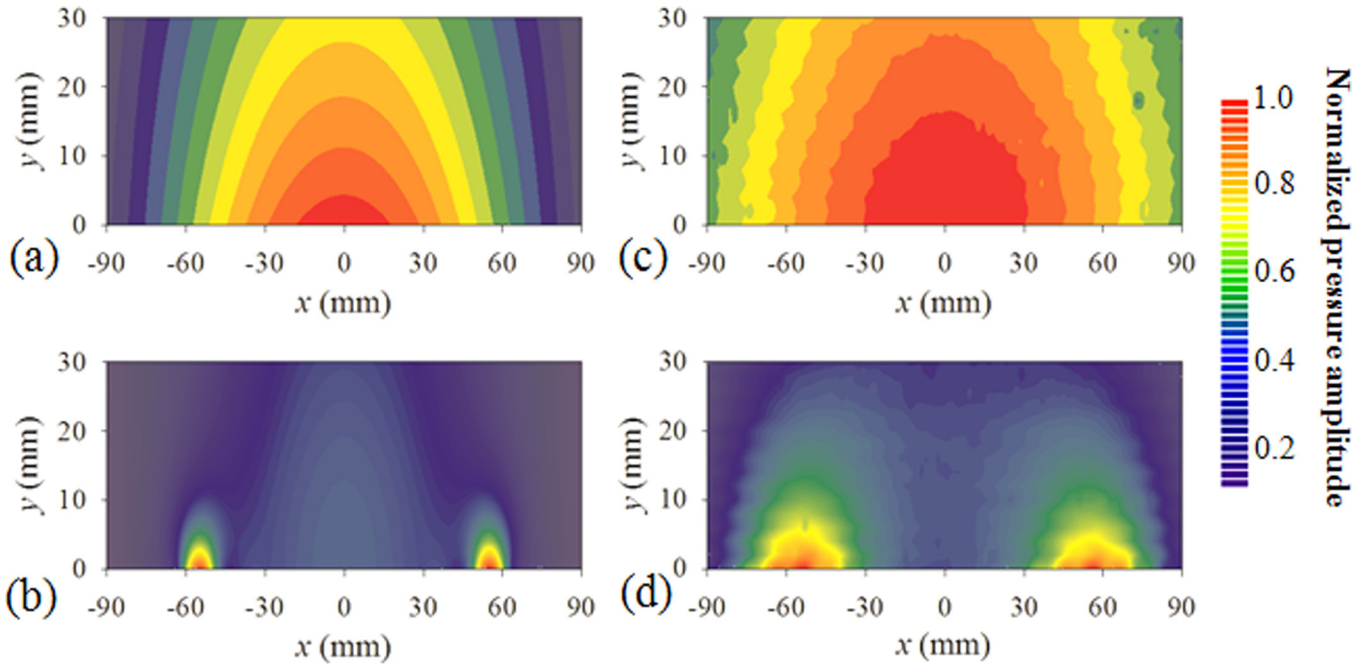

FIG. 9. (Color online) Simulation (a) and (b) and experiment (c) and (d) results of normalized pressure amplitudes in the image region in the absence (a) and (c) and presence (b) and (d) of the holey-structured lens when two loudspeakers separated by 110 mm are placed in front of the lens with the distance 2 mm.

noise, the signals received by the microphone are filtered by band-pass filters. The LABVIEW program is coded to deal with the signal processing and control of stepping motors.

Figure 8 shows both simulation and experiment results of the normalized pressure amplitudes in the line taken 2 mm behind the lens when one source with the operating frequency 905 Hz (its wavelength in air is 380 mm) is placed in front of the lens at the distance $w = 2$ mm. It can be found that there is only one lobe observed from the pressure amplitude profile in the plane parallel to the output side of the lens, and the basis of the lobe of this profile becomes zero in the location far from the peak position. So the resolution of the lens can be defined as the full width at half maximum (FWHM) of pressure amplitudes, which is $\lambda/5.2$ according to simulation results. The measured FWHM is about $\lambda/4.1 \approx 92.7$ mm; the possible reason for this difference is the moderate acoustic loss when acoustic wave penetrates the lens.

When two sources with the separation 110 mm ($\approx \lambda/3.5$) are located in front of the lens at the distance $w = 2$ mm, the amplitude distributions of pressure fields in the image region are displayed in Figs. 9(b) and 9(d), which are obtained, respectively, by numerical simulation and experimental measurement. Two bright spots can be observed in the near field adjacent to the lens by which two sources can be clearly distinguished. Because the subwavelength information of the two sources is stored in near-field evanescent waves, one cannot distinguish two sources in the far field when the lens is absent as illustrated in Figs. 9(a) and 9(c).

Figure 10 shows the pressure amplitudes in the line taken 2 mm behind the lens for various distances between the source and the lens, $w = 2$, 4, and 6 mm. It can be found that the imaging effect becomes worse when the source is located further away from the lens. This is because evanescent waves decay rapidly; their wave amplitudes become very small when they travel a long distance before reaching the lens. The overall profile between simulation and experiment coincides very well, but there are some discrepancies of pressure amplitudes between them. The reason of the discrepancy may be that the small waveguide used as the source in numerical simulation is not able to describe very accurately the loudspeaker performance, so that the wave interference between the waveguides cannot result in an evident drop around the center region of the amplitude curves.

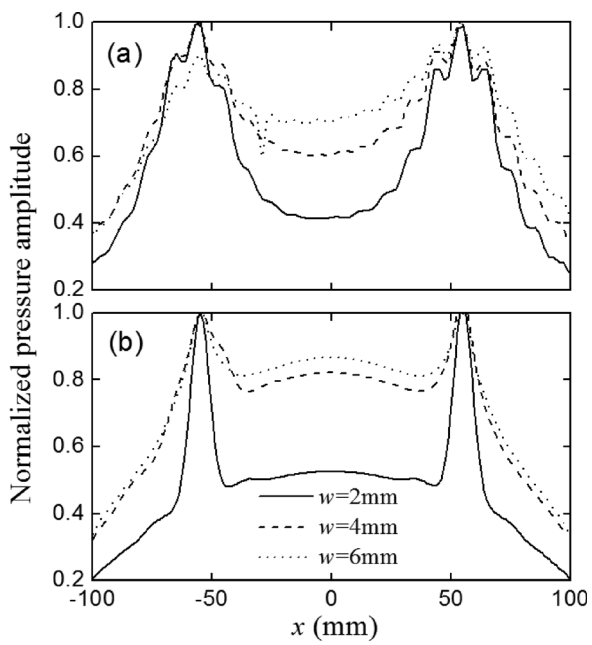

FIG. 10. (a) Experiment and (b) simulation results of normalized pressure amplitudes in the line taken 2 mm behind the lens for various distances between the source and the lens, 2, 4, and 6 mm.

The preceding experimental results clearly demonstrate that the designed lens can indeed interact with evanescent waves by coupling to the tunneling modes and then transfer them to the far side of the lens to form acoustic super-resolution images. In practice, evanescent waves may appear as parts of scattered fields coming from unknown objects. When they are captured by acoustic imaging system with help of the designed lens, high-resolution images can then be achieved.

IV. CONCLUSIONS

This work studies a holey-structured metamaterial lens capable of acoustic subwavelength imaging beyond the diffraction limit. The lens prevents evanescent waves from decaying based on the resonant tunneling mechanism. An advantage of the lens is that the tunneling frequency can be changed by modulating the diameter ratio of internal cylindrical holes, while the lens thickness remains unchanged. Its behavior is distinct from that of the holey-structured lens based on the FP resonance, the imaging frequency of which is controlled by the lens thickness. The analytic model has been constructed to evaluate transmission properties of evanescent waves through the structured lens. Experimental results demonstrate that the proposed lens is easily fabricated and capable of distinguishing two sources separated in the distance below the diffraction limit at the tunneling frequencies.

ACKNOWLEDGMENT

This work was supported by the National Natural Science Foundation of China (Grant Nos. 10832002, 11172038, 11072031, and 11221202), the National Basic Research Program of China (Grant No. 2011CB610302), and Program for New Century Excellent Talents in University (Grant No. NCET-11-0794).

[1]Z. Liu, X. Zhang, Y. Mao, Y. Y. Zhu, Z. Yang, C. T. Chan, and P. Sheng, "Locally resonant sonic materials," Science **289**(5485), 1734–1736 (2000).
[2]N. Fang, D. Xi, J. Xu, M. Ambati, W. Srituravanich, C. Sun, and X. Zhang, "Ultrasonic metamaterials with negative modulus," Nat. Mater. **5**(6), 452–456 (2006).
[3]S. Zhang, L. Yin, and N. Fang, "Focusing ultrasound with an acoustic metamaterial network," Phys. Rev. Lett. **102**(19), 194301 (2009).
[4]M. Ambati, N. Fang, C. Sun, and X. Zhang, "Surface resonant states and superlensing in acoustic metamaterials," Phys. Rev. B **75**(19), 195447 (2007).
[5]K. Deng, Y. Ding, Z. He, H. Zhao, J. Shi, and Z. Liu, "Theoretical study of subwavelength imaging by acoustic metamaterial slabs," J. Appl. Phys. **105**(12), 124909 (2009).
[6]F. Liu, F. Cai, S. Peng, R. Hao, M. Ke, and Z. Liu, "Parallel acoustic near-field microscope: A steel slab with a periodic array of slits," Phys. Rev. E **80**(2), 026603 (2009).
[7]J. Zhu, J. Christensen, J. Jung, L. Martin-Moreno, X. Yin, L. Fok, X. Zhang, and F. J. Garcia-Vidal, "A holey-structured metamaterial for acoustic deep-subwavelength imaging," Nat. Phys. **7**(1), 52–55 (2011).
[8]X. Zhou and G. Hu, "Superlensing effect of an anisotropic metamaterial slab with near-zero dynamic mass," Appl. Phys. Lett. **98**(26), 263510 (2011).
[9]A. Liu, X. Zhou, G. Huang, and G. Hu, "Super-resolution imaging by resonant tunneling in anisotropic acoustic metamaterials," J. Acoust. Soc. Am. **132**(4), 2800–2806 (2012).
[10]H. Jia, M. Ke, R. Hao, Y. Ye, F. Liu, and Z. Liu, "Subwavelength imaging by a simple planar acoustic superlens," Appl. Phys. Lett. **97**(17), 173507 (2010).
[11]S. H. Lee, C. M. Park, Y. M. Seo, Z. G. Wang, and C. K. Kim, "Acoustic metamaterial with negative density," Phys. Lett. A **373**(48), 4464–4469 (2009).
[12]S. Yao, X. Zhou, and G. Hu, "Investigation of the negative-mass behaviors occurring below a cut-off frequency," New J. Phys. **12**(10), 103025 (2010).
[13]S. Yao, X. Zhou, and G. Hu, "Experimental study on negative effective mass in a 1D mass–spring system," New J. Phys. **10**(4), 043020 (2008).
[14]A. Sukhovich, L. Jing, and J. H. Page, "Negative refraction and focusing of ultrasound in two-dimensional phononic crystals," Phys. Rev. B **77**(1), 014301 (2008).
[15]D. Torrent and J. Sánchez-Dehesa, "Anisotropic mass density by radially periodic fluid structures," Phys. Rev. Lett. **105**(17), 174301 (2010).
[16]L. E. Kinsler, A. R. Frey, A. B. Coppens, and J. V. Sanders, *Fundamentals of Acoustics*, 4th ed. (Wiley, New York, 1999), 526 pp.